robotics

MDPI

Article

Variable Damping Actuator Using an Electromagnetic Brake for Impedance Modulation in Physical Human–Robot Interaction

Zahid Ullah [1], Ronnapee Chaichaowarat [2,*] and Witaya Wannasuphoprasit [1]

[1] Department of Mechanical Engineering, Chulalongkorn University, 254 Phayathai Road, Pathumwan, Bangkok 10330, Thailand; 6471005421@student.chula.ac.th (Z.U.); witaya.w@chula.ac.th (W.W.)
[2] International School of Engineering, Chulalongkorn University, 254 Phayathai Road, Pathumwan, Bangkok 10330, Thailand
* Correspondence: ronnapee.c@chula.ac.th

Abstract: Compliance actuation systems are efficient and safe, drawing attention to their development. However, compliance has caused bandwidth loss, instability, and mechanical vibration in robotic systems. Variable physical damping was introduced to address these issues. This paper presents a technique for obtaining variable damping properties using an electromagnetic brake. The relationship mapping of the voltage and the braking torque is studied and applied to the variable damping concept. A new model is proposed to demonstrate the actuation system performance gained by introducing physical damping. The experimental setup comprises an electromagnetic brake and a motor with an integrated controller for speed control and torque feedback. The motor provides the motion, while the electromagnetic brake replicates the damping through a friction mechanism. The variable damping concept was evaluated experimentally using a 1-degree-of-freedom rotational system. Experimental results show that the proposed concept can generate the desired mechanical damping with a high degree of fidelity.

Keywords: actuators; electromagnetic brake; friction mechanism; variable physical damping

Citation: Ullah, Z.; Chaichaowarat, R.; Wannasuphoprasit, W. Variable Damping Actuator Using an Electromagnetic Brake for Impedance Modulation in Physical Human–Robot Interaction. *Robotics* **2023**, *12*, 80. https://doi.org/10.3390/robotics12030080

Academic Editors: Xiaowei Huang, Wenjie Ruan and Xingyu Zhao

Received: 8 May 2023
Revised: 30 May 2023
Accepted: 1 June 2023
Published: 4 June 2023

1. Introduction

In past decades, the concept of variable impedance actuators (VIA) has received greater attention from researchers, as many of the novel applications involving human-robot interactions and an unknown environment are not achieved by classical stiff actuators [1]. Considering the safety of robots, the concept of variable impedance control was introduced. In improving the safety, compliance, and efficiency of human-robot interactions, variable impedance control has been considered one of the main approaches [2]. In 1985, impedance modulation was proposed by Hogan to achieve the desired spring-damping dynamics [3]. This method is considered one of the most powerful compliant control approaches. Most robots developed in the past exhibited stiff dynamics because of the actuation approach actuated by electric DC or brushless motors coupled with a high transmission gear ratio and controlled with high-gain controllers [4,5]. These actuators work within a specific area to avoid human interaction, which can be dangerous because of their limited safety performance and, in turn, sets important limitations related to the safety and efficiency of these actuators or traditional stiff robots and their ability to interact with the environment. The introduction of physical compliance within a robot's structure is a new and widely used trend in modern industry [6]. This approach has been used because of the incompatibility of the classical stiff and heavy manipulators with high-gain controllers for operation near the physical human interaction with the surrounding environment.

Friction dampers were studied in [7] for modal and optimal control; however, this approach neglects variations in friction parameters, as seismic dampers are not subject to persistent oscillations, and damper actuator dynamics were not considered in comparison to structural dynamics. In [8], the author explored electrorheological (ER) damper control,

where damper dynamics were represented using a transfer function coupling dissipation torque to input voltage. Because the velocity change was not continuous, linear modeling was possible. As with robots with compliant joints that may have extremely dynamic movements, changes in speed and friction due to wear and heating must be accounted for [9–11]. A neural-network-based approach for adaptive vibration control using ER dampers that ignores damper actuator dynamics is presented in [12].

Dampers are categorized into three types based on the amount of power they need to operate (passive, active, or semi-active). Passive dampers offer a set amount of damping and are the most basic option; nevertheless, from a robotic aspect, they may not be effective when energy efficiency is needed or when the damping level must be varied to accommodate load configuration changes [13]. Purely active dampers, however, may need a large amount of energy to operate and are only valid within the closed-loop bandwidth of the controlled system [14]. In addition, in position, velocity, or torque-controlled actuators and compliant actuators with low joint physical damping show a clear antiresonance on the motor side [15]. Thus, a solution based solely on active damping will reach its limits across resonance, as the motor controllability is very low near this frequency. Unlike active systems, which can adjust the stiffness and damping components of the mechanical impedance, semi-active devices [16,17] can only control the latter component. Compared to active dampers, these types of dampening devices often need substantially less energy while retaining the adaptability of active dampers and providing inherent passivity and dependability [18].

The concern for safety in human-robot interactions has led to the development of a new actuator system with a semi-active damper and passive compliance. This system has been referred to as a variable physical damping (VPD) actuator [19]. Variable dampers are extensively deployed in robotics and mechanical systems. Recently, variable dampers have been employed in compliant actuators to improve the physical human-robot interaction [20–24]. Variable stiffness actuators were proposed to overcome the drawbacks arising from passive elasticity, i.e., unpremeditated oscillations that can lead to inaccuracies in stability and motion [25,26]. These issues are also addressed in other VIA strategies [22,27,28]. To overcome the limitations caused by physical compliance, friction-based semi-active dampers were introduced in the compliance actuators. The aforementioned information leads to the conclusion that using an actuation approach that can offer passive compliance and VPD (i.e., a semi-active damper) can form an effective means for the development of robots that can interact with their surroundings safely and robustly while still exhibiting good dynamic performance and accuracy. However, this idea is not easily realized, particularly when we consider the high integration density required in robotics systems.

It was proposed that magneto-rheological (MR) fluid dampers and variable friction dampers be used in a complaint system in parallel with a spring that could contribute damping to the system [29,30]. Some MR fluid dampers are also used in civil, structure, and automation suspension systems [31–36]. In addition, [37] presented a variable damping mechanism based on electrical inductance effects on a DC motor.

Furthermore, some damping modules have been developed using ER fluid [38,39]; the main drawback of these actuators is that they provide less friction. In addition, using an ER fluid brake requires many components, which makes the assembly more complex and difficult. Moreover, ER fluid brakes increase in size, weight, and cost. In [40], the author proposed a hybrid damping actuator that uses two motors and encoders that make the design bulky. Variable impedance actuation has been the subject of several studies, with an emphasis on software control [41–50] for mechatronic design [51–54].

On the basis of the preceding discussion, we suggest an electromagnetic (EM) brake with high friction, a simple design, low cost, and compact size for a variable damping actuation system. In this work, we demonstrate the successful implementation of a 1-degree-of-freedom rotational system of a variable damping actuator comprising its entire realization process. We analyzed the interaction torque, studied the relationship between the voltage and torque, and applied the concept to a variable damping actuator.

Thus, the novelty and main contribution of this work is the development and subsequent experimental evaluation of an improved model by designing and developing an actuator incorporating an EM brake damper. The EM brake controls the brake force as it corresponds to the speed to replicate damping behavior. The EM brake adjusts the damping and provides the damping as desired. The implemented damper is a fast and strong friction mechanism with a large dissipative capacity that may be adjusted to change the apparent damping of the system.

This paper is organized as follows. Section 2 introduces the design concept, the operating principle, and the mechanical design of the variable damping actuator. Section 3 shows the EM brake characterization. Section 4 describes the experimental setup and discusses the results obtained from the improved model. Section 5 presents the results of different damping torque tests, while Section 6 summarizes the key findings.

2. The Variable Damping Actuator Concept

2.1. Operating Principle

A variable damping actuator using an EM brake provides variable damping properties by adjusting the brake friction torque. The experimental setup comprises a brake and a motor having a built-in encoder. The brake operates by applying a DC voltage across its terminals. When voltage is applied to the coil of the EM brake, the magnetic flux attracts the armature to the face of the brake, and the resistive friction force between the brake stator and the brake rotor is increased. The friction force is increased and decreased by varying the voltage across its terminal. At 0 V, the stator and rotor of the EM brake are not in mechanical contact, and the distance between them is 0.3 mm. The rotor is connected to the coupling, which is rotating, and thus, the torque is transmitted from the rotor to the brake.

2.2. Conceptual Design

To study the variable damping concept, the experimental setup comprised a motor and an EM brake. A conceptual design of the overall system is shown in Figure 1. The motor is driven by supplying the voltage source. The actuator used the SINFONIA EM brake NB-0.3 (Tokyo, Japan). The experimental setup was developed to validate the VPD concept.

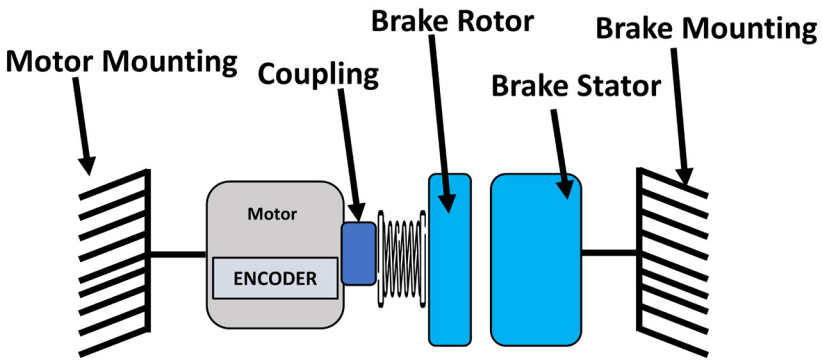

Figure 1. Schematic of the variable damping actuation system.

2.3. Mechanical Design

The CAD design of the experimental setup to study the variable damping actuator system is shown in Figure 2. The motor is rotated by providing the voltage, while the EM brake provides the physical damping as controlled friction. In this arrangement, the EM brake is parallel to the motor. The developed mechanical setup of the assembled actuator is shown in Figure 3. The system comprised two main assemblies, the motor assembly and the EM brake assembly. An AK70-10 motor with a 10:1 reduction ratio was used, combined with a planetary gear solution.

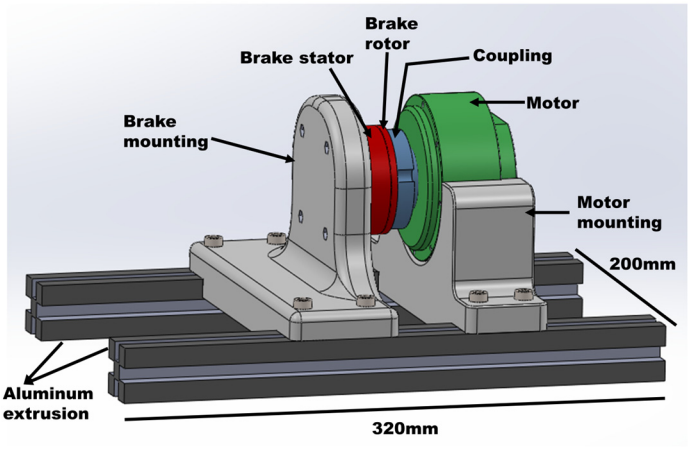

Figure 2. CAD design of the experimental setup to study the variable damping actuator system.

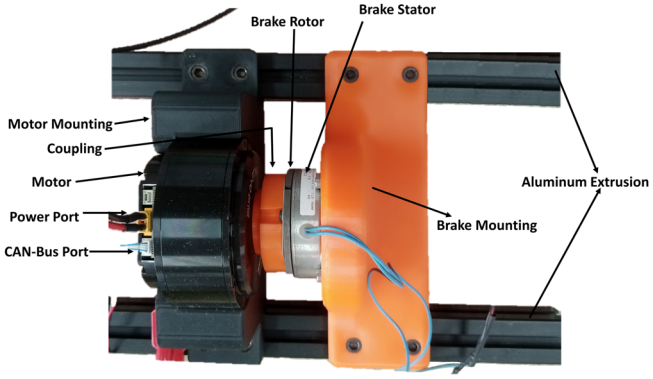

Figure 3. Developed variable damping actuator using an electromagnetic brake.

The actuator generates a torque referred to as τ_{ref}. This torque can be modeled by (1). The brake was integrated with the actuator with the help of a custom 3D-printed coupling. The 4040-type standard square-shaped aluminum extrusion was used to mount the motor and the EM brake. The motor and the EM brake were held firmly by 3D custom print mount holders. The entire system was mounted onto the aluminum extrusion and clamped tightly with the help of the clampers. The experimental setup to study the variable damping system was built, as shown in Figure 3. The actuator used a planetary geared motor to support the rotation of the system, while the EM brake was used to mimic the damping behavior. The actuator used an AK70-10 motor with a peak torque of 24.8 Nm, and 521 g of weight was used.

The control system was implemented on the VPD actuator experimental setup. The position of the motor is denoted as θ. The motor rotates with angular velocity $\dot{\theta}$, and the EM brake is adjusted to mimic the damping behavior as corresponds to the change in the angular velocity of the motor. To operate the system, the actuator was programmed once to receive the command, and the desired damping torque was achieved. The CANBUS shield was used for communication, while the motor was responsible for the rotation. The DC motor driver (PRIK-THAI V.2) was used to generate the PWM signal. The torque of the motor can be represented as (1):

$$\tau_{ref} = K_p(\theta_{des} - \theta_{act}) + K_d\left(\dot{\theta}_{des} - \dot{\theta}_{act}\right) + \tau_i \quad (1)$$

where τ_{ref} is the reference torque of the motor, K_p is the stiffness of the motor, K_d is the damping of the motor, θ_{des} is the desired position of the motor, θ_{act} is the actual position of the motor, $\dot{\theta}_{des}$ is the desired angular velocity of the motor, $\dot{\theta}_{act}$ is the actual angular velocity of the motor, and τ_i is the current torque computed from the motor current.

The reference torque of the motor is computed from the desired position, angular velocity, stiffness, and damping. After receiving the desired command, the motor controller returns the actual position, the angular velocity, and the current torque of the motor. Without any external load, the current torque is the result of the motor-gearbox friction (both static and viscous friction). In this paper, the current torque is one important feedback from the motor controller that indicates the combination of the motor-gearbox friction and the damping torque generated by the electromagnetic brake.

3. Electromagnetic Brake Characterization

This section provides the details of the EM brake characterization. The brake used was a SINFONIA (Tokyo, Japan) pancake-type EM brake NB-0.3. The rated voltage of the brake was 24 volts DC, the maximum speed at idling was 9500 r/min, and the max speed at engaging or braking was 8000 r/min. The installation space between the friction surface of the brake stator and the armature plate of the brake rotor was fixed at 0.3 mm so that the brake rotor could freely rotate when the magnetic field was deactivated. To study the characterization of the brake, the EM brake was integrated with a motor with the help of custom design 3D CAD coupling. In these studies, an AK70-10 motor served as a velocity source. A DC 24 V power supply was used as an input voltage source to the motor and brake.

The voltage torque profile is crucial for the variable damping mechanisms. A voltage signal is applied to the motor and the EM brake. In response to the activation of the magnetic field, the spring plate of the brake rotor undergoes deformation, and the brake rotor moves in an axial direction, bringing it into contact with the friction surface of the brake stator. The motor was rotated at constant velocities $\dot{\theta} = 1, 2, 3,$ and 4 rad/s, and at each voltage, the output torque was observed 30 times to obtain the average value. The input voltage to the EM brake was progressively changed from 0 to 24 VDC as it was provided by the DC power supply (E3630A) manufactured by Hewlett-Packard (Roseville, CA, USA) (see Figure 4). This power supply could accommodate a maximum current of 0.5 A [55]. Figure 5 plots the braking torque as a function of the input brake voltage. The braking torque does not substantially change when the voltage is less than 5 V, but it can be linearly estimated when the input voltage is greater than 5 V. In addition, similar results are obtained for the torque against each input velocity.

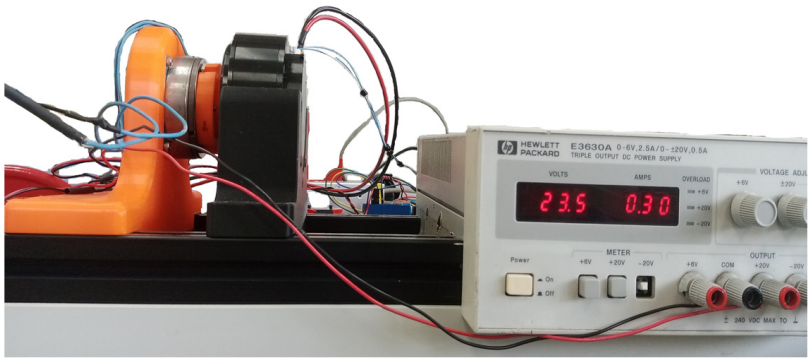

Figure 4. Experimental setup for the electromagnetic brake characterization using a power supply system.

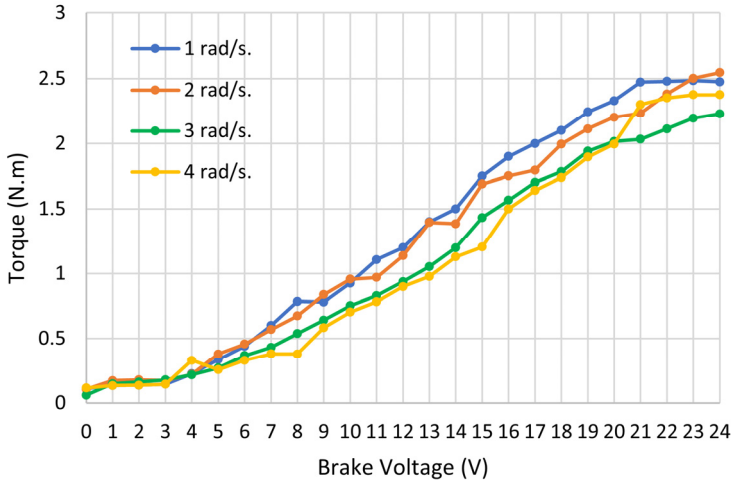

Figure 5. Electromagnetic braking torque increases with the voltage observed at different rotational velocities.

The torque profile can also be verified by providing a PWM commanded to the PRIK-THAI V.2 (Bangkok, Thailand) drive circuit. The relationship mapping the PWM and the voltage was studied and applied to the brake. The PWM signal ranges from 0 to 255, where PWM 0 and 255 correspond to 0 and 24 V, respectively. The maximum voltage was controlled through the PWM signal from the microcontroller (Arduino UNO) (Ivrea, Italy). A major advantage of using PRIK-THAI V.2 was that the voltage was controlled automatically by a microcontroller, eliminating the need for manual adjustments. Torque varying against PWM was observed against rotational velocities $\dot{\theta} = 1, 2, 3,$ and 4 rad/s, and the output torque against each velocity was analyzed, as shown in Figure 6. Similar to the voltage–torque plot in Figure 5, the torque has no substantial change when the PWM value is less than 50 but can be linearly estimated when the PWM value is greater than 50. The PWM–torque plot is shown in Figure 6.

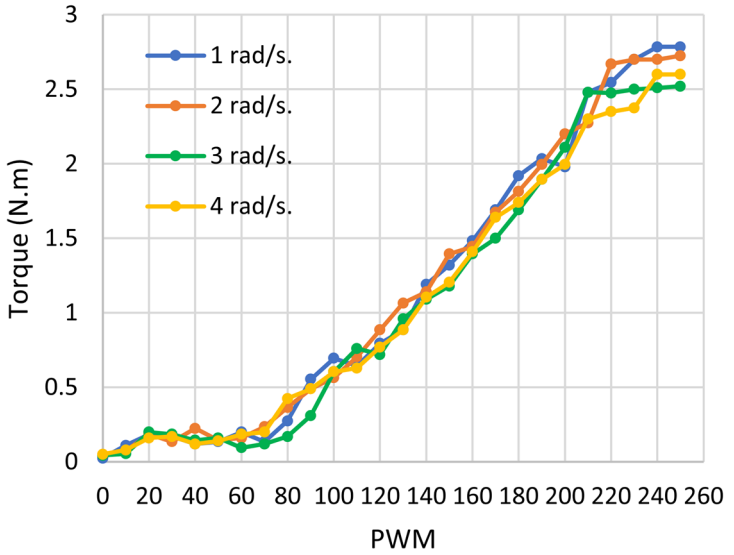

Figure 6. Electromagnetic bake torque varies against the PWM commanded to PRIK-THAI V.2 drive circuit.

4. Variable Damping Experiment Verification

4.1. Experimental Setup and Procedure

To study the performance of the actuator, various experiments were conducted to validate the variable damping concept. The EM braking torque was controlled to mimic the behavior of the variable damper with a damping coefficient, c. The velocity of the motor

increases linearly with time, as shown in Figure 7a. Torque increases with time in Figure 7b, but initially, it does not increase linearly with speed.

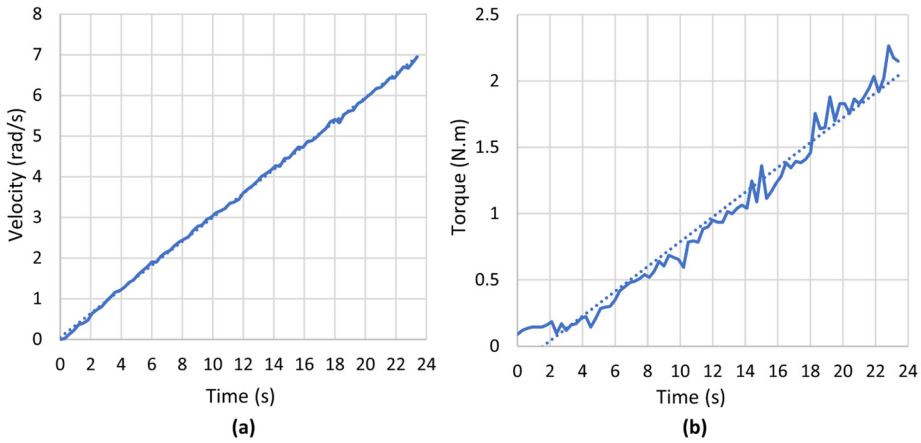

Figure 7. (**a**) Velocity increases linearly with time. (**b**) Torque varies against time. The torque does not change substantially from 0 to 5 s. After 5 s, the torque can be linearly estimated. Linear approximations are shown by the dashed lines.

The initial chaotic behavior of the torque was due to the linear mapping of the PWM and torque. To clearly show that the torque does not change when the PWM is lower than a certain value, the torque is plotted against the PWM in Figure 8 (blue plot). The PWM signal at the start of the experiment had an unsubstantial effect on the brake. The braking torque can be estimated from (2). As per the conventional model of the braking torque in (2), a nonuniform region caused the torque to fluctuate. The region of chaotic behavior can be clearly seen in Figures 7b and 8. This chaotic behavior destabilizes the system.

$$\tau_{brake} = m(PWM) \tag{2}$$

where τ_{brake} is the braking torque, m is the slope of the VPD system, and PWM is the signal provided to the brake.

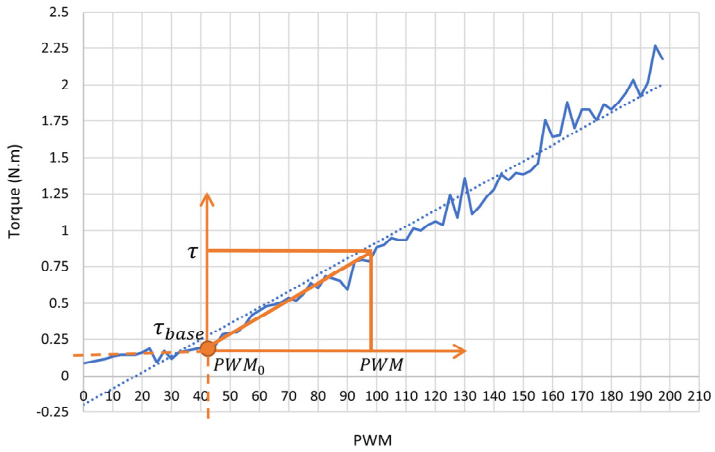

Figure 8. The torque increases with PWM. The chaotic behavior in the torque can be observed in blue when the PWM is less than 50. When the PWM value is greater than 50, the torque tends to be linear. Linear approximation is shown by the dashed line.

Before studying the performance of the variable damping actuator, we needed to study the torque behavior that changes with different velocities; for this reason, experiments for two motor damping coefficients, $k_d = 1$ Nms/rad and $k_d = 4$ Nms/rad, were performed.

The speed was commanded to the motor through Arduino UNO. The actual velocity was retrieved from the motor through the Arduino. Then, the desired torque was computed, and the corresponding PWM was commanded to the brake. The brake creates a frictional force and generates the rotating torque. Initially, the damping coefficient (k_d) of the motor was set to 1 Nms/rad. From the experiments, it was observed that for the lower motor damping coefficient ($k_d = 1$ Nms/rad), the actual and desired velocities differ, and a large velocity error can be observed in Figure 9a.

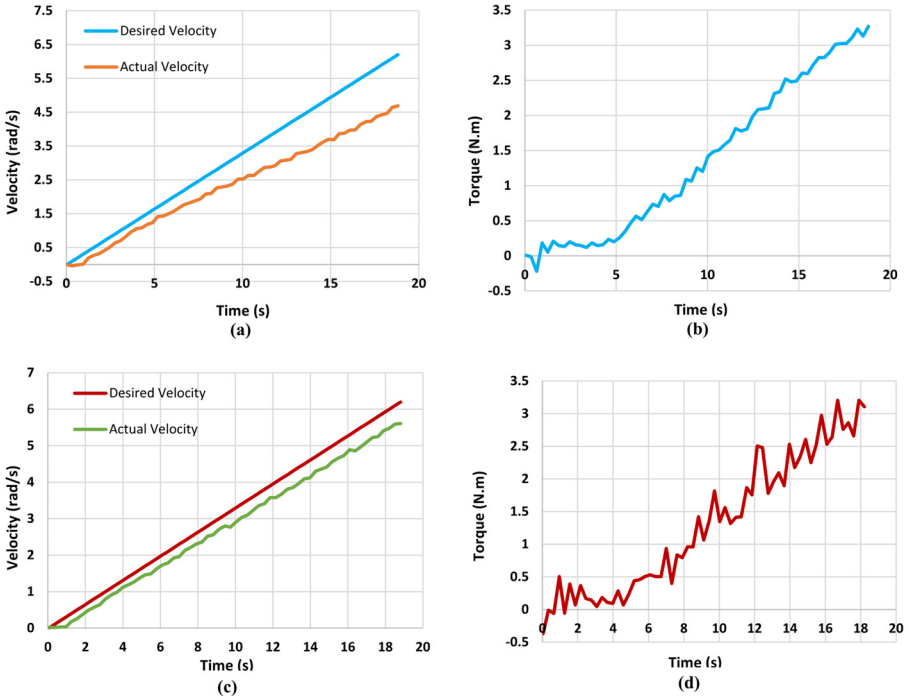

Figure 9. (**a**) Velocity of motor at k_d = 1 Nms/rad. (**b**) Torque of motor at k_d = 1 Nms/rad. (**c**) Velocity of motor at k_d = 4 Nms/rad. (**d**) Torque of motor at k_d = 4 Nms/rad.

Figure 9b shows that for $k_d = 1$ Nms/rad, although a larger velocity error is observed, the torque fluctuation is low. To track the desired value of velocity, the motor damping coefficient (k_d) must be high enough to reach the desired velocity. In the second experiment, the motor damping coefficient was set to $k_d = 4$ Nms/rad. The result in Figure 9c shows that for $k_d = 4$ Nms/rad, the velocity tracking is very good, and the velocity error is small, but fluctuations in the torque are high, as observed in Figure 9d. From the experiments, we conclude that a compromise must be made between speed and torque. The braking torque can be estimated from (3).

$$\tau_{ref} = k_d\left(\dot{\theta}_{des} - \dot{\theta}_{act}\right) \tag{3}$$

Equation (3) shows that the lower motor damping value ($k_d = 1$ Nms/rad) has an unsubstantial effect on the velocity when the difference in velocity is larger, but the higher motor damping value ($k_d = 4$ Nms/rad) results in a minimal difference in velocity. Differences in velocities are seen in Figure 9a,c.

4.2. Improved Model

This section provides an improved model for the variable damping actuator by eliminating the region where the torque is essentially constant. We introduced the corrected mapping of the PWM signal and torque. The signal where the torque is essentially constant is represented as PWM_0 in (4), whereas τ_{base} is the offset value of the torque. The improved model (5) has the advantage of starting the torque at the point where the torque does not

fluctuate. To clearly describe the improved model, a graphical representation is depicted in Figure 8 (using an orange color).

$$\tau - \tau_{base} = m(PWM - PWM_o) \tag{4}$$

$$\tau = m(PWM - PWM_o) + \tau_{base} \tag{5}$$

To verify the improved model experimentally, two brake damping coefficients, $c = 0.1$ Nms/rad and $c = 0.25$ Nms/rad, were taken, and experiments were performed. The experimental results show that the velocity increases linearly with time, as shown in Figure 10a, and the region of nonuniformity was removed, as shown in Figure 10b.

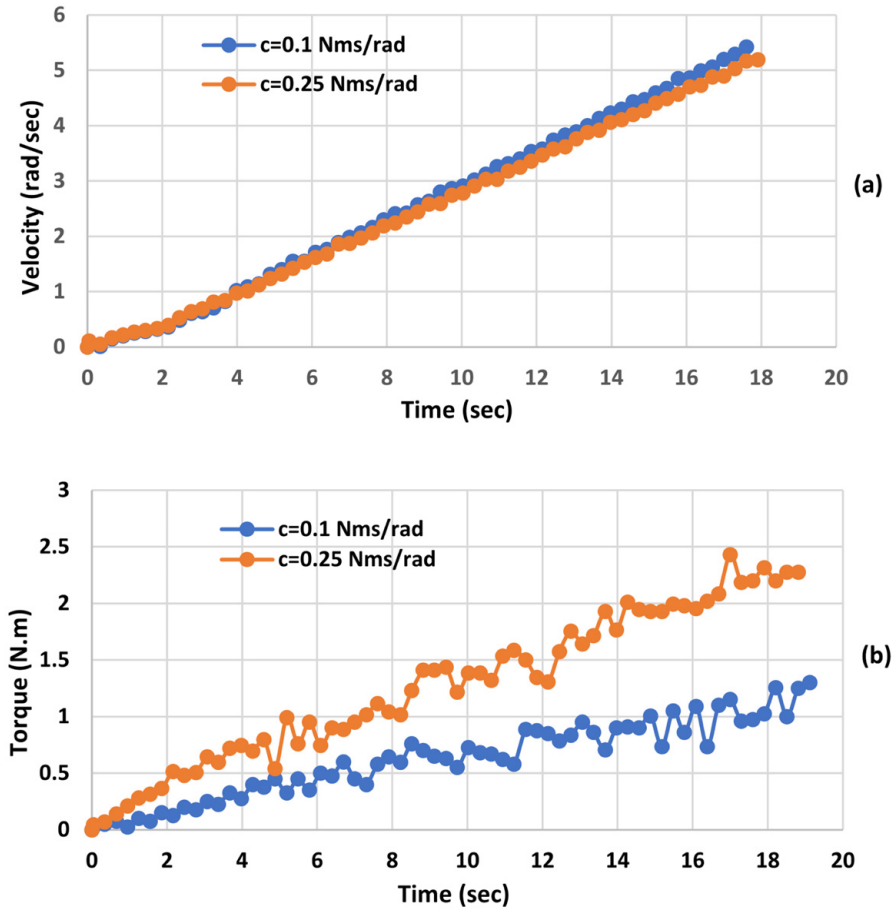

Figure 10. Improved Model. (**a**) The velocity increases linearly with time. (**b**) The torque varying against time shows linear trends.

5. Damping Torque Validation

This experimental setup aims to produce variable damping and validate the concept through step and sinusoidal response. To validate the variable damping concept, experiments were performed for the damping coefficients $c1 = 0.1$ Nms/rad, $c2 = 0.25$ Nms/rad, and $c3 = 0.4$ Nms/rad. In each case, the system successfully generated the desired damping with high fidelity. Figure 11 shows the generated variable damping torque plot.

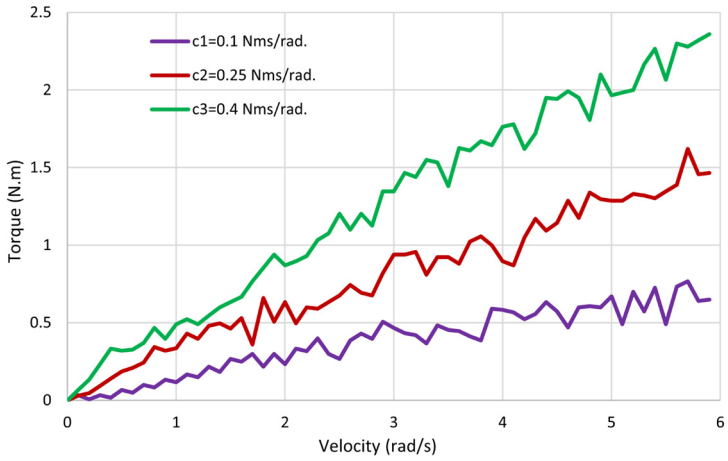

Figure 11. Damping torque validation. Torque–velocity plot for three damping levels.

5.1. Step Reference

To determine the actuator performance against the positive and negative step responses, the torque response is plotted in Figure 12. The ideal torque varies from 0.2 to 0.6 N·m, while in the real system, the torque slightly fluctuates, and the system's output response is delayed. The fluctuation in the torque is due to the stick-slip effect. Similar fluctuations and delays were also observed in [38]. In the intervals of 0 to 2 s, the damping coefficient of the brake was zero; in 2 to 4 s, the damping coefficient was set to c = 0.25 Nms/rad; and finally, in 4 to 6 s, the damping coefficient was again set to c = 0 Nms/rad. Ideally, when there is no damping coefficient, the torque must be zero. A small amount of torque (i.e., 0.2 N·m) was observed because of the friction in the gearbox system. The speed of the system was held constant at 2 rad/s during the experiment. A delay of 200 ms was observed to change the signal from a positive step reference to a negative step reference. Sampling data points were collected every 20 ms and 200 ms. Fluctuations in the torque were observed for the data points of the 20 ms sampling period. No significant difference was observed between the systems except for the fluctuations. A small delay was observed in the negative step response signal for the system with a 200 ms sampling period. The experimental results proved that the system successfully tracked the ideal torque trajectory.

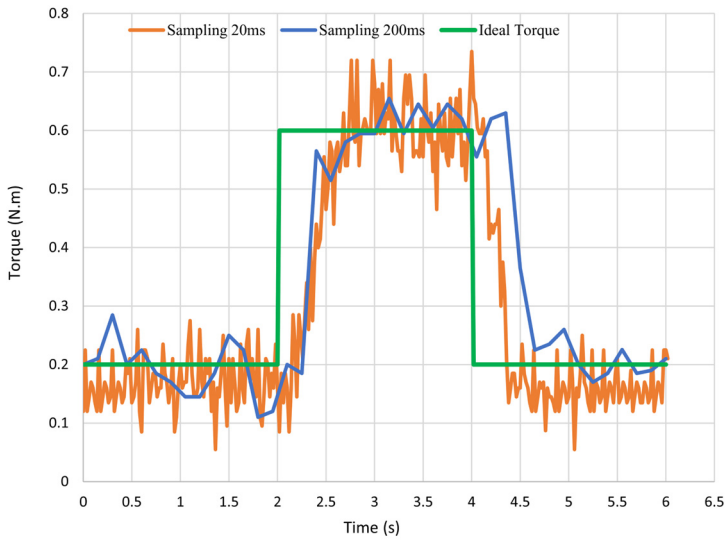

Figure 12. Torque response to positive and negative step commands.

5.2. Sinusoidal Reference

The sinusoidal response of the system was verified at a high frequency, $f = 0.5$ Hz, and a low frequency, $f = 0.1$ Hz. The damping coefficient was set to 2 Nms/rad for both experiments. The high frequency is probably equivalent to being struck with a hammer. The hammer hitting time can be assumed to be 2 s. The response of the system on tracking the sinusoidal references during 2 s periods (for 0.5 Hz) and 10 s periods (for 0.1 Hz) was validated experimentally, and the system performances at low and high frequencies are shown in Figures 13 and 14, respectively. The position of the system changed sinusoidally. The velocity, which is the time derivative of the position, also varied sinusoidally. During these experiments, the EM brake was actuated to behave as a rotary damper, and the data were recorded for two periods. The result shows that the system can track the ideal torque with good performance.

The actual velocity obtained from the motor controller was computed from the encoder position and contained fluctuation. It is worth noting that the velocity profile is smoother at the higher frequency (Figure 14), where the motor is controlled to change the position continuously. At the lower frequency (Figure 13), the stick-slip effect causes an uneven velocity profile. The actual torque observed from the experiment is the combination of the variable damping torque generated by the EM brake (based on the non-smooth velocity) and the nonlinear motor-gear box friction, which is the major source of the torque discrepancy (especially under the significant effect of stick-slip phenomenon at the lower frequency).

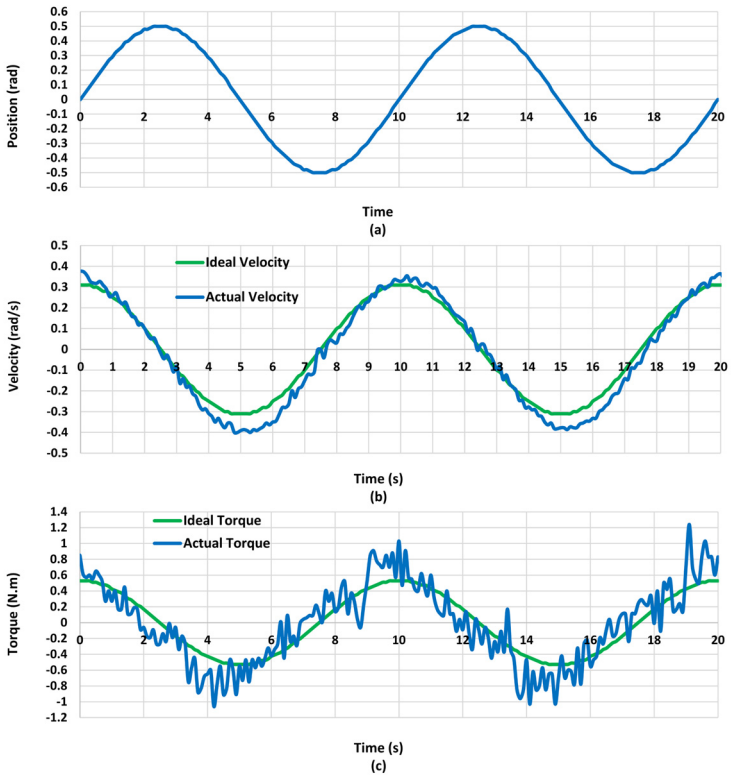

Figure 13. Sinusoidal response of the system at low frequency $f = 0.1$ Hz. (**a**) Sinusoidal position of the system. (**b**) Velocity tracking following a sinusoidal reference of the system at 0.1 Hz. (**c**) Torque tracking following a sinusoidal reference of the system at 0.1 Hz.

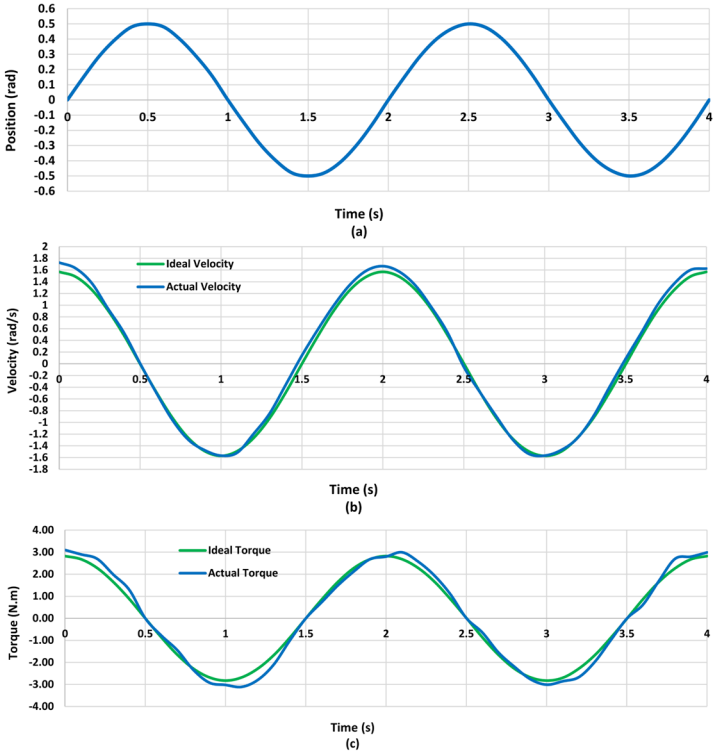

Figure 14. Sinusoidal response of the system at high frequency $f = 0.5$ Hz. (**a**) Sinusoidal position of the system. (**b**) Velocity tracking following a sinusoidal reference of the system at 0.5 Hz. (**c**) Torque tracking following a sinusoidal reference of the system at 0.5 Hz.

6. Conclusions and Future Work

This paper introduced the novel concept of voltage and PWM mapping for a variable damping actuator. The actuator incorporated an EM brake. The actuator's mechanical design and the mechatronic components were explained in depth. The system's dynamic responses and torque were characterized through experimental tests. A single-degree-of-freedom rotational system was used to test the proposed variable damper mechanism. The measured characteristics of the damper aligned with the design calculations, validating the design approach through experimentation. In addition, the results confirmed that the unit is fast and powerful enough to achieve the desired damping. Further work will concentrate on integrating the variable damping actuator into a macro–mini linear actuator [38] for active body weight support systems.

Author Contributions: Conceptualization, Z.U. and R.C.; methodology, Z.U. and R.C.; software, Z.U. and R.C.; validation, Z.U. and R.C.; formal analysis, Z.U. and R.C.; investigation, Z.U. and R.C.; resources, R.C. and W.W.; data curation, Z.U. and R.C.; writing—original draft preparation, Z.U. and R.C.; writing—review and editing, Z.U., R.C. and W.W.; visualization, Z.U., R.C. and W.W.; supervision, R.C. and W.W.; project administration, R.C.; funding acquisition, R.C. All authors have read and agreed to the published version of the manuscript.

Funding: This research project is partially funded by the Second Century Fund (C2F), Chulalongkorn University, Thailand, and the Thailand Science Research and Innovation Fund, Chulalongkorn University (IND66210017).

Data Availability Statement: The data presented in this study are available on request from the corresponding author. The data are not publicly available due to privacy.

Conflicts of Interest: The authors declare no conflict of interest.

References

1. Vanderborght, B.; Albu-Schaeffer, A.; Bicchi, A.; Burdet, E.; Caldwell, D.G.; Carloni, R.; Catalano, M.; Eiberger, O.; Friedl, W.; Ganesh, G.; et al. Variable impedance actuators: A review. *Rob. Auton. Syst.* **2013**, *61*, 1601–1614. [CrossRef]
2. Sun, T.; Peng, L.; Cheng, L.; Hou, Z.G.; Pan, Y. Stability-guaranteed variable impedance control of robots based on approximate dynamic inversion. *IEEE Trans. Syst. Man Cybern. Syst.* **2021**, *51*, 4193–4200. [CrossRef]
3. Hogan, N. Impedance Control Part1-3. *J. Dyn. Syst. Meas. Control.* **1985**, *107*, 1–24. [CrossRef]
4. Wannasuphoprasit, W.; Chanphat, S. T-Cobot: Transformable Collaborative Robot. In Proceedings of the 2005 ASME International Mechanical Engineering Congress and Exposition. Dynamic Systems and Control, Parts A and B, Orlando, FL, USA, 5–11 November 2005; pp. 1689–1696.
5. Wannasuphoprasit, W.; Gillespie, R.B.; Colgate, J.E.; Peshkin, M.A. Cobot control. In Proceedings of the IEEE International Conference on Robotics and Automation, Albuquerque, NM, USA, 25 April 1997; Volume 4, pp. 3571–3576.
6. Kashiri, N.; Medrano-Cerda, G.A.; Tsagarakis, N.G.; Laffranchi, M.; Caldwell, D. Damping control of variable damping compliant actuators. In Proceedings of the 2015 IEEE International Conference on Robotics and Automation (ICRA), Seattle, WA, USA, 26–30 May 2015; pp. 850–856.
7. Lu, L.Y.; Chung, L.L.; Lin, G.L. A general method for semi-active feedback control of variable friction dampers. *J. Intell. Mater. Syst. Struct.* **2004**, *15*, 393–412. [CrossRef]
8. Nakamura, T.; Saga, N. Viscous control of homogeneous ER fluid using a variable structure control. *IEEE/ASME Trans. Mechatron.* **2005**, *10*, 154–160. [CrossRef]
9. Lakatos, D.; Petit, F.; Albu-Schäffer, A. Nonlinear oscillations for cyclic movements in human and robotic arms. *IEEE Trans. Robot.* **2014**, *30*, 865–879. [CrossRef]
10. Chaichaowarat, R.; Kinugawa, J.; Kosuge, K. Cycling-enhanced Knee Exoskeleton Using Planar Spiral Spring. In Proceedings of the 2018 40th Annual International Conference of the IEEE Engineering in Medicine and Biology Society (EMBC), Honolulu, HI, USA, 18–21 July 2018; pp. 3206–3211.
11. Chaichaowarat, R.; Kinugawa, J.; Seino, A.; Kosuge, K. A Spring—Embedded Planetary—Geared Parallel Elastic Actuator. In Proceedings of the 2020 IEEE/ASME International Conference on Advanced Intelligent Mechatronics (AIM), Boston, MA, USA, 6–9 July 2020.
12. Hidaka, S.; Ahn, Y.K.; Morishita, S. Adaptive vibration control by a variable damping dynamic absorber using er fluid. *J. Vib. Acoust. Trans. ASME* **1999**, *121*, 373–378. [CrossRef]
13. Tzou, H.S.; Wan, G.C. Distributed structural dynamics control of flexible manipulators -I. Structural dynamics and distributed viscoelastic actuator. *Comput. Struct.* **1990**, *35*, 669–677. [CrossRef]
14. Lew, J.Y.; Moon, S.M. A simple active damping control for compliant base manipulators. *IEEE/ASME Trans. Mechatron.* **2001**, *6*, 305–310. [CrossRef]
15. Siciliano, B.; Khatib, O. *Springer Handbook of Robotics*; Springer: Berlin/Heidelberg, Germany, 2016; ISBN 9783319325521.
16. Yadmellat, P.; Kermani, M.R. Adaptive modeling of a magnetorheological clutch. *IEEE/ASME Trans. Mechatron.* **2014**, *19*, 1716–1723. [CrossRef]
17. Shafer, A.S.; Kermani, M.R. On the feasibility and suitability of mr fluid clutches in human-friendly manipulators. *IEEE/ASME Trans. Mechatron.* **2011**, *16*, 1073–1082. [CrossRef]
18. Sun, J.Q.; Jolly, M.R.; Norris, M.A. Passive, adaptive and active tuned vibration absorbers—A survey. *J. Mech. Des. Trans. ASME* **1995**, *117*, 234–242. [CrossRef]
19. Laffranchi, M.; Tsagarakis, N.G.; Caldwell, D.G. A variable physical damping actuator (VPDA) for compliant robotic joints. In Proceedings of the 2010 IEEE International Conference on Robotics and Automation, Anchorage, AK, USA, 3–7 May 2010; pp. 1668–1674.
20. Tsagarakis, N.G.; Laffranchi, M.; Vanderborght, B.; Caldwell, D.G. A compact soft actuator unit for small scale human friendly robots. In Proceedings of the 2009 IEEE International Conference on Robotics and Automation, Kobe, Japan, 12–17 May 2009; pp. 4356–4362.
21. Pratt, G.A.; Williamson, M.M. Series elastic actuators. In Proceedings of the 1995 IEEE/RSJ International Conference on Intelligent Robots and Systems. Human Robot Interaction and Cooperative Robots, Pittsburgh, PA, USA, 5–9 August 1995; Volume 1, pp. 399–406.
22. Okada, M.; Ban, S.; Nakamura, Y. Skill of Compliance with Controlled Charging/Discharging of Kinetic Energy. In Proceedings of the International Conference on Robotics & Automation (ICRA)Automation (ICRA), Washington, DC, USA, 11–15 May 2002; pp. 2455–2460.
23. Niu, Z.; Awad, M.I.; Shah, U.H.; Boushaki, M.N.; Zweiri, Y.; Seneviratne, L.; Hussain, I. Towards Safe Physical Human-Robot Interaction by Exploring the Rapid Stiffness Switching Feature of Discrete Variable Stiffness Actuation. *IEEE Robot. Autom. Lett.* **2022**, *7*, 8084–8091. [CrossRef]
24. Hussain, I.; Albalasie, A.; Awad, M.I.; Tamizi, K.; Niu, Z.; Seneviratne, L.; Gan, D. Design and Control of a Discrete Variable Stiffness Actuator with Instant Stiffness Switch for Safe Human-Robot Interaction. *IEEE Access* **2021**, *9*, 118215–118231. [CrossRef]
25. Chaichaowarat, R.; Nishimura, S.; Krebs, H.I. Design and Modeling of a Variable-Stiffness Spring Mechanism for Impedance Modulation in Physical Human Robot Interaction. In Proceedings of the 2021 IEEE International Conference on Robotics and Automation (ICRA), Xi'an, China, 30 May–5 June 2021; pp. 7052–7057.

26. Javadi, A.; Chaichaowarat, R. Position and stiffness control of an antagonistic variable stiffness actuator with input delay using super-twisting sliding mode control. *Nonlinear Dyn.* **2022**, *111*, 5359–5381. [CrossRef]
27. Catalano, M.; Grioli, G.; Garabini, M.; Belo, F.W.; Di Basco, A.; Tsagarakis, N.; Bicchi, A. A Variable Damping module for Variable Impedance Actuation. In Proceedings of the ICRA, St. Paul, MN, USA, 14–18 May 2012; pp. 2666–2672.
28. Catalano, M.G.; Grioli, G.; Garabini, M.; Bonomo, F.; Mancini, M.; Tsagarakis, N.; Bicchi, A. VSA-CubeBot: A modular variable stiffness platform for multiple degrees of freedom robots. In Proceedings of the 2011 IEEE International Conference on Robotics and Automation, Shanghai, China, 9–13 May 2011; pp. 5090–5095.
29. Yoon, S.S.; Kang, S.; Kim, S.J.; Kim, Y.H.; Kim, M.; Lee, C.W. Safe Arm with MR-based Passive Compliant Joints and Visco-elastic Covering for Service Robot Applications. In Proceedings of the International Conference on Intelligent Robots and Systems, Las Vegas, NV, USA, 27–31 October 2003.
30. Chew, C.M.; Hong, G.S.; Zhou, W. Series damper actuator system based on MR fluid damper. *Robotica* **2006**, *24*, 699–710. [CrossRef]
31. Laffranchi, M.; Chen, L.; Kashiri, N.; Lee, J.; Tsagarakis, N.G.; Caldwell, D.G. Development and control of a series elastic actuator equipped with a semi active friction damper for human friendly robots. *Rob. Auton. Syst.* **2014**, *62*, 1827–1836. [CrossRef]
32. Sukhnandan, R.; Dai, K.; Webster-Wood, V. A Magnetorheological Fluid-based Damper Towards Increased Biomimetism in Soft Robotic Actuators. In Proceedings of the 2022 International Conference on Robotics and Automation (ICRA), Philadelphia, PA, USA, 23–27 May 2022; pp. 11445–11451.
33. Wang, Q.; Ahmadian, M.; Chen, Z. A novel double-piston magnetorheological damper for space truss structures vibration suppression. *Shock Vib.* **2014**, *2014*. [CrossRef]
34. Oh, J.S.; Choi, S.B. Ride quality control of a full vehicle suspension system featuring magnetorheological dampers with multiple orifice holes. *Front. Mater.* **2019**, *6*, 8. [CrossRef]
35. Zhu, X.; Jing, X.; Cheng, L. Magnetorheological fluid dampers: A review on structure design and analysis. *J. Intell. Mater. Syst. Struct.* **2012**, *23*, 839–873. [CrossRef]
36. Gołdasz, J.; Sapiński, B. *Insight into Magnetorheological Shock Absorbers*; Springer International Publishing: Cham, Switzerland, 2015; ISBN 9783319132334.
37. Radulescu, A.; Howard, M.; Braun, D.J.; Vijayakumar, S. Exploiting variable physical damping in rapid movement tasks. In Proceedings of the 2012 IEEE/ASME International Conference on Advanced Intelligent Mechatronics (AIM), Kaohsiung, Taiwan, 11–14 July 2012; pp. 141–148.
38. Chaichaowarat, R.; Nishimura, S.; Krebs, H.I. Macro-Mini Linear Actuator Using Electrorheological-Fluid Brake for Impedance Modulation in Physical Human-Robot Interaction. *IEEE Robot. Autom. Lett.* **2022**, *7*, 2945–2952. [CrossRef]
39. Li, J.; Jin, D.; Zhang, X. An Electrorheological Fluid Damper for Robots. In Proceedings of the 1995 IEEE International Conference on Robotics and Automation, Nagoya, Japan, 21–27 May 1995; pp. 2631–2636.
40. Sarakoglou, I.; Tsagarakis, N.G.; Caldwell, D.G. Development of a hybrid actuator with controllable mechanical damping. In Proceedings of the 2014 IEEE International Conference on Robotics and Automation (ICRA), Hong Kong, China, 31 May–7 June 2014; pp. 1078–1083.
41. Kemper, K.; Koepl, D.; Hurst, J. Optimal passive dynamics for torque/force control. In Proceedings of the 2010 IEEE International Conference on Robotics and Automation, Anchorage, AK, USA, 3–7 May 2010; pp. 2149–2154.
42. Fumagalli, M.; Ivaldi, S.; Randazzo, M.; Natale, L.; Metta, G.; Sandini, G.; Nori, F. Force feedback exploiting tactile and proximal force/torque sensing: Theory and implementation on the humanoid robot iCub. *Auton. Robot.* **2012**, *33*, 381–398. [CrossRef]
43. Abe, K.; Suga, T.; Fujimoto, Y. Control of a biped robot driven by elastomer-based series elastic actuator. *Int. Work. Adv. Motion Control. AMC* **2012**.
44. Zollo, L.; Siciliano, B.; Laschi, C.; Teti, G.; Dario, P. An experimental study on compliance control for a redundant personal robot arm. *Rob. Auton. Syst.* **2003**, *44*, 101–129. [CrossRef]
45. Serio, A.; Grioli, G.; Sardellitti, I.; Tsagarakis, N.G.; Bicchi, A. A decoupled impedance observer for a variable stiffness robot. In Proceedings of the 2011 IEEE International Conference on Robotics and Automation, Shanghai, China, 9–13 May 2011; pp. 5548–5553.
46. Flacco, F.; De Luca, A. Residual-based stiffness estimation in robots with flexible transmissions. In Proceedings of the 2011 IEEE International Conference on Robotics and Automation, Shanghai, China, 9–13 May 2011; pp. 5541–5547.
47. Frémy, J.; Ferland, F.; Lauria, M.; Michaud, F. Force-guidance of a compliant omnidirectional non-holonomic platform. *Rob. Auton. Syst.* **2014**, *62*, 579–590. [CrossRef]
48. Grioli, G.; Bicchi, A. A non-invasive, real-time method for measuring variable stiffness. *Robot. Sci. Syst.* **2011**, *6*, 89–96.
49. Flacco, F.; De Luca, A.; Sardellitti, I.; Tsagarakis, N.G. On-line estimation of variable stiffness in flexible robot joints. *Int. J. Rob. Res.* **2012**, *31*, 1556–1577. [CrossRef]
50. Hussain, I.; Albalasie, A.; Awad, M.I.; Gan, D. Modeling, identification, and control of a discrete variable stiffness actuator (DVSA). *Actuators* **2019**, *8*, 50. [CrossRef]
51. Fumagalli, M.; Barrett, E.; Stramigioli, S.; Carloni, R. The mVSA-UT: A miniaturized differential mechanism for a continuous rotational variable stiffness actuator. In Proceedings of the 2012 4th IEEE RAS & EMBS International Conference on Biomedical Robotics and Biomechatronics (BioRob), Rome, Italy, 24–27 June 2012; pp. 1943–1948.

52. Enoch, A.; Sutas, A.; Nakaoka, S.; Vijayakumar, S. BLUE: A bipedal robot with variable stiffness and damping. In Proceedings of the 2012 12th IEEE-RAS International Conference on Humanoid Robots (Humanoids 2012), Osaka, Japan, 29 November–1 December 2012; pp. 487–494.
53. Van Ham, R.; Vanderborght, B.; Van Damme, M.; Verrelst, B.; Lefeber, D. MACCEPA, the mechanically adjustable compliance and controllable equilibrium position actuator: Design and implementation in a biped robot. *Rob. Auton. Syst.* **2007**, *55*, 761–768. [CrossRef]
54. Chanthasopeephan, T.; Jarakorn, A.; Polchankajorn, P.; Maneewarn, T. Impact reduction mobile robot and the design of the compliant legs. *Rob. Auton. Syst.* **2014**, *62*, 38–45. [CrossRef]
55. Chaichaowarat, R.; MacHa, V.; Wannasuphoprasit, W. Passive knee exoskeleton using brake torque to assist Stair Ascent. In Proceedings of the 2020 IEEE Region 10 Conference (Tencon), Osaka, Japan, 16–19 November 2020; pp. 1165–1170.